

The Search for a Primordial Magnetic Field

Dai G. Yamazaki

National Astronomical Observatory of Japan, Mitaka, Tokyo 181-8588, Japan

Toshitaka Kajino

National Astronomical Observatory of Japan, Mitaka, Tokyo 181-8588, Japan

*Department of Astronomy, Graduate School of Science, The University of Tokyo, Hongo
7-3-1, Bunkyo-ku, Tokyo 113-0033, Japan*

Grant J. Mathews

*Department of Physics, Center for Astrophysics, University of Notre Dame, Notre
Dame, IN 46556, U.S.A.*

Kiyotomo Ichiki

Department of Physics and Astrophysics, Nagoya University, Nagoya 464-8602, Japan

Abstract

Magnetic fields appear wherever plasma and currents can be found. As such, they thread through all scales in Nature. It is natural, therefore, to suppose that magnetic fields might have been formed within the high temperature environments of the big bang. Such a primordial magnetic field (PMF) would be expected to arise from and/or influence a variety of cosmological phenomena such as inflation, cosmic phase transitions, big bang nucleosynthesis, the cosmic microwave background (CMB) temperature and polarization anisotropies, the cosmic gravity wave background, and the formation of large-scale structure. In this review, we summarize the development of theoretical models for analyzing the observational consequences of a PMF. We also summarize the current state of the art in the search for observational evidence of a PMF. In particular we review the framework needed to calculate the effects of a PMF power spectrum on the CMB and the development of large scale structure. We summarize the current constraints on the PMF amplitude B_λ and the power spectral index n_B and discuss prospects for better determining these quantities in the near future.

Keywords: Cosmic microwave background, Large scale structures, primordial magnetic field

1. Introduction

It is well known that magnetic fields influence many physical processes over a broad range of scales in the universe. It is natural, therefore, to suppose that currents and associated magnetic fields could arise from the flow of material in the high temperature environment of the big bang. Such a primordial magnetic field (PMF) would be expected to manifest itself in the cosmic microwave background (CMB) temperature and polarization anisotropies [1, 2, 3, 4, 5, 6, 7, 8, 9, 10, 11, 12, 13, 14, 15, 16, 17, 18, 19, 20, 21, 22, 23, 24, 25], and also in the formation of large-scale structure (LSS) [26, 27, 28]. These studies have pointed out that the effects of a PMF are not negligible if the PMF had a field strength $B_\lambda \sim 1.0$ nG on ~ 1 Mpc scales at the epoch of photon last scattering, $z \sim 1100$. Therefore, it is important to constrain the PMF parameters by cosmological observations. The purpose of this review is to summarize progress in the development of the calculational techniques to deduce such constraints from existing observational data. First, however, we motivate this endeavor with a brief discussion of why one thinks there might be a PMF from both theoretical grounds and observations of galaxy clusters.

1.1. Generation models of a PMF

Many authors have been actively studying the origin of cosmological primordial magnetic fields. Possible generation mechanisms have recently been reviewed in detail by [29]. In brief, such primordial fields are expected to have random distribution of orientations and field strengths. If the PMF has a nearly scale invariant spectrum like the primary scalar spectrum, one of the best models is an origin from vector potentials generated during the inflation epoch [30, 31, 32]. Several authors have proposed that a PMF with a bluer spectrum could have been produced during one of the subsequent cosmological phase transitions [33, 34, 35, 36]. A magnetic field could also have been generated during or after the epoch of photon last scattering ($z \lesssim 1100$) by vorticities in the cosmological fluid [37, 38, 39]. Since each model for the generation of the PMF involves different length scales, the spectral index of the PMF power spectrum, n_B , will depend upon which is the correct model

for the generation of the PMF. Therefore, constraining n_B phenomenologically can lead to constraints on the epoch for the generation of the PMF.

1.2. Observational evidence for a PMF

Observations of synchrotron emission [40] and Faraday rotation [41, 42, 43] in galaxy clusters all indicate the presence of magnetic fields on large scales. Moreover, magnetic fields with a strength of $B \sim 1.0 \mu\text{G}$ have been detected in several galaxy clusters [41, 42, 43]. Simulations of such cluster magnetic fields may require [44] the existence of a primordial seed magnetic field.

Since the diffusion time of a magnetic field in galaxy clusters is much longer than the age of the universe, such a magnetic field is "frozen-in" to the ionized fluids [2]. The energy density of the baryon fluid scales as $\rho_b \propto a^{-3}$ while the magnetic energy density scales as $\rho_B \propto a^{-4}$. Therefore, one can relate the strength of the magnetic field energy density to the energy density of the cosmic baryon fluid $B^3 \propto \rho_b^2$. If clusters of galaxies collapse nearly isotropically relative to the background space, an observed magnetic field of $B \sim 1.0 \mu\text{G}$ in galaxy clusters now corresponds to a PMF of order $\sim 1.0 \text{ nG}$ at the epoch of photon last scattering near $z \sim 1100$.

1.3. Constraint on a PMF by Cosmological observations

As noted above there is a large difference between the strength of any cosmological magnetic field during the generation epoch and that which could be detected at the present time. In most currently proposed theoretical scenarios, the generation of a PMF involves some physical process that generates current in the early universe *before* the epoch of photon last scattering. However, cosmological observation determine the CMB anisotropies and the matter power spectrum on various cosmological scales *during* and *after* the epoch of photon last scattering. It is therefore timely and desirable to construct precise theoretical models with which to analyze the CMB anisotropies and the large-scale-structure (LSS) matter power spectrum as obtained in present and soon to be obtained cosmological observations. The purpose of this review is to summarize the development of such models.

2. Models for the Generation of a PMF

The origin of a cosmological primordial magnetic field has been an area of active research by many authors [See [29] for an excellent review]. The proposed models can be divided into three classes which we briefly summarize.

First, however, note that the cosmological magnetic field damps as

$$B_0 \propto a^{-2}, \quad (1)$$

where a is the cosmological scale factor. In order to avoid confusion, therefore, it is best refer to a comoving PMF field strength B_0 scaled to the present-day value on some length scale (taken here to be 1 Mpc), i.e. we write

$$B_0 = B(\tau) \times \left(\frac{a(\tau)}{a_0(\tau)} \right)^2, \quad (2)$$

where τ is the conformal time defined by the differential $d\tau = a dt$.

2.1. Inflation

During the epoch of inflation small quantum perturbations are believed to have been extended and enlarged into those of super horizon scales [45]. Since spacetime in normal inflation is conformally flat [45], the spacetime and any associated electromagnetic field are independent and invariant to a conformal transformation. Therefore, unless this invariance to a conformal transformation is broken, a magnetic field cannot be generated by the expanding spacetime [30, 31, 32].

In [30], however, it was assumed that the electromagnetic field and the gravitational field interacted in such a way as to break the invariance of the electromagnetic fields to a conformal transformation. They then showed that a magnetic field could be generated by quantum perturbations. There are several means to naturally break such invariance. For example, the strength of a PMF generated by an electromagnetic tensor of the dilaton type, has been estimated to be $\sim 1\text{nG}$ and $\sim 10^{-5}\text{nG}$ by [32] and [46], respectively.

2.2. EW transition/QCD transition

Cosmological phase transitions could also produce a PMF with a bluer spectrum [33, 34, 35, 36] than that of inflation models. For example, bubbles of a new lower temperature phase can be made at the cosmological quark-hadron [47] or electroweak [48] phase transitions. As those bubbles collide and percolate, the baryon symmetry is broken leading to the generation of a magnetic field [47]. The strength of the magnetic field generated at these epochs has been estimated to be $\sim 10^{-7}\text{nG}$ for fields generated by the quark-hadron transition [47] and $\sim 10^{-14} - 10^{-8}\text{nG}$ for the electroweak transition [48].

2.3. Decoupling and afterward

Magnetic field generation can also occur on smaller scales during or after the epoch of photon last scattering ($z < 1000$) [38, 37, 39]. If there were eddies before the recombination epoch, they could generate a PMF [39]. Even without turbulent eddies, the known CMB temperature fluctuations imply the generation of at least some magnetic primordial field. Since protons have mass and photons do not, photons scatter electrons differently than protons. This difference induces electric currents as they fall in and out of gravitational potentials. These electric fields can generate a magnetic field of about 10^{-9} nG at 1 Mpc. [39].

3. Constraints on the Physics of a PMF

In this section we briefly introduce that the effects of a PMF on Big-Bang Nucleosynthesis (BBN), the Gravitational Wave Background (GWB), the Cosmic Microwave Background (CMB) and Large Scale Structure (LSS). We then qualitatively discuss constraints on the PMF parameters deduced from each observation. Following that we shall quantitatively review how the PMF parameters are constrained by multiple cosmological observations.

Of course one does not really know *a priori* the spectrum of cosmological magnetic fields. As a starting point, however, it is natural to presume that one can characterize the PMF parameters in the same way one does for photons, i.e. by a power-law spectrum of PMF energy density fluctuations on different wave numbers k , i.e.

$$P(B_k) \propto k^{n_B} \quad , \quad (3)$$

where $P(B_k)$ denotes the power in magnetic field energy density on the scale of wave number k and n_B is a spectral index.

In previous work {e.g. Refs.[5, 12]} approximate power law spectra were utilized to describe a PMF. These approximate spectra have been very convenient for exploring the qualitative effects of a PMF on various physical phenomena. However, in this approximation one cannot obtain quantitatively accurate results. For example, one could not accurately constrain the parameters of a PMF from cosmological observations. In Yamazaki et al. (2008)[15], however, a power law formulation for a PMF was developed without approximation (See Appendix A for details). Using this formula, we have been able to calculate the effects of a PMF by accounting for the time

evolution of the cut off scale to high accuracy. Also, we have constructed a numerical program without approximation, for studying the effects of a PMF on the cosmological perturbations.

Since our main purpose is to review how parameters of the PMF are constrained by cosmological observations, we first make a brief explanation of the various ways in which a PMF affects cosmology. The reader who wishes to understand PMF effects in more detail is referred to the following papers regarding the CMB: Ref.[2, 5, 12, 15, 23], LSS: Ref.[26, 27, 28, 17, 24], and the GWB: Ref.[49]. After reviewing the observational constraints we will conclude with a discussion of the constraints upon possible origins of a PMF based on the present constraints on the PMF parameters from fits to the available observations.

3.1. Constraints from BBN and the GWB

The balance between the expansion rate of the universe and various particle reaction rates has important effects on the nucleosynthesis of light elements in the big-bang. Moreover, since the energy density of the GWB, ρ_{GWB} , contributes to the total energy density of the universe, the expansion rate is affected by the GWB. Therefore, we can indirectly constrain the energy density ρ_{GWB} from the light element primordial abundances inferred from observations of deuterium (D), ^3He , ^4He , and ^7Li . Following [50] one can relate the upper limit to the energy density in gravity waves to the upper limit on the effective number of neutrino flavors N_ν present during BBN:

$$\int_0^\infty d \log(\nu) h_0^2 \Omega_{\text{GWB}}(\nu) \leq 5.6 \times 10^{-6} (N_\nu - 3) \quad , \quad (4)$$

where ν is the frequency of the GWB, h_0 is the Hubble parameter (in units of $100 \text{ km s}^{-1} \text{ Mpc}^{-1}$), Ω_{GWB} is the ratio of the energy density of the GWB ρ_{GWB} to the critical density of the universe ρ_c .

The upper limit to the number of neutrino flavors N_ν is constrained from a variety of observations. If one only utilizes a comparison between BBN and the inferred primordial abundances of deuterium (D) and helium (^4He) in the standard big bang one obtains [51]:

$$N_\nu = 3.14_{-0.65}^{+0.70} \text{ at } 68\% \text{ CL} \\ (2.49 \leq N_\nu \leq 3.84 \text{ at } 68\% \text{ CL}) \quad . \quad (5)$$

Alternatively, if one considers constraints from the WMAP [52, 53, 54, 55] CMB power spectrum analysis including Luminous Red Galaxies (LRG) [56, 57] and the Hubble constant, H_0 measurements, this limit increases to [58]

$$3.45 \leq N_\nu \leq 5.01 \text{ at 68\% CL .} \quad (6)$$

Or, if one also includes baryon acoustic oscillations (BAO) in the analysis this limit becomes [58]

$$3.46 \leq N_\nu \leq 5.20 \text{ at 68\% CL .} \quad (7)$$

An analysis that also includes constraints from Type Ia supernovae (SN) $WMAP + BAO + SN + HST$ leads to [58]

$$2.90 \leq N_\nu \leq 5.90 \text{ at 68\% CL .} \quad (8)$$

Therefore, depending upon which constraint is adopted, one can rewrite Eq.(12) as:

$$\int_0^\infty d \log(\nu) h_0^2 \Omega_{\text{GWB}}(\nu) \leq 4.7 \times 10^{-6} \text{BBN, D and } ^4\text{He}, \quad (9)$$

$$\leq 1.13 \times 10^{-5} (WMAP + LRG + H_0), \quad (10)$$

$$\leq 1.23 \times 10^{-5} (WMAP + BAO + H_0), \quad (11)$$

$$\leq 1.62 \times 10^{-5} (WMAP + BAO + SN + HST). \quad (12)$$

Caprini and Durrer [49] have analyzed the generation of a GWB from fluctuations in the PMF. They then used the BBN constraints on the GWB to place surprisingly strong constraints on the parameters characterizing a PMF. Following [49], we have recalculated the GWB upper limits on the PMF field strength as a function of spectral index for a PMF formed during different epochs. These are shown¹ in Fig.1. The right part of this figure is an expanded plot for spectral indices n_B from -3 to -2.5. The green, blue, and red lines on this plot are the upper limits to a PMF generated during big-bang nucleosynthesis, the electroweak transition, or the inflation epoch,

¹Caprini and Durrer (2004) quoted field strength for a comoving scale of galaxies $\lambda = 0.1$ Mpc, however our results are quoted for galaxy cluster scales $\lambda = 1$ Mpc.

respectively. For this plot we adopt the WMAP constraint on N_ν from the *WMAP + BAO + SN + HST* analysis [58].

If the PMF were generated during inflation, the power should be nearly scale invariant ($n_B \sim -3$) [2]. In this case, the PMF parameters are not constrained strongly by the associated GWB. For example, PMF fields strengths as large as $B_\lambda \sim 10^{-7}\text{G}$ are allowed for a spectral index of $n_B \sim -3$ (right panel of Fig.1). As we review later, the constraint on the PMF strength from various cosmological observations is less than several nano Gauss. Therefore, if the PMF were generated during the inflation epoch and the PMF power spectrum is nearly scale-invariant, the PMF strength is not constrained very much by this method.

On the other hand, if the PMF were generated after the inflation epoch it has a bluer spectrum (smaller spectral index) and is better constrained by the GWB. One can deduce from the left panel of Fig.1, that the strength of a PMF generated during the EW epoch has an upper limit of order 10^{-11}G , 10^{-15}G or 10^{-20}G for $n_B = -2, -1$ or 0 , respectively. Similarly, if the PMF were generated during the BBN epoch, the upper limit of the PMF strength is constrained to be order 10^{-10}G , 10^{-14}G or 10^{-18}G for $n_B = -2, -1$ or 0 , respectively.

Furthermore, since the upper limit on the PMF amplitude, B_λ^{up} , depends upon the effective number of neutrinos N_ν allowed in the early universe:

$$B_\lambda^{\text{up}} \propto \sqrt{N_\nu - 3}, \quad (13)$$

the constraints on the PMF parameters strongly depend upon independent observations which constrain N_ν .

There has also been an attempt to constrain the PMF field strength from direct measurements of limits to the present cosmological GWB. [59] has deduced the constraint $B_\lambda < 4 \times 10^{-7}\text{G}$ at 1 Mpc and $B_\lambda < 9 \times 10^{-11}\text{G}$ at 100 Mpc from the LIGO S5 data [60].

3.2. Constraints from the CMB

For a PMF of order 1.0-10 nG at the surface of photon last scattering, the total energy density in the PMF is much smaller than that of the temperature fluctuations of the CMB (called the T -mode, where T denotes the total scalar temperature). Therefore, we can treat the energy density of a PMF as a first order perturbation and assume a stiff source for the time evolution [2]. That is, all back reactions from the fluid onto the magnetic field can be discarded

because they are second order perturbations. In this case, we can also assume that the conductivity of the primordial plasma is very large and that the electric field is negligible, i.e. $E \sim 0$. This "frozen-in" condition is a very good and useful approximation [2].

Recently, the CMB polarization power spectra have been observed by several projects. This has allowed for more precise constraints [23, 61, 62] on the PMF and other cosmological parameters. For clarity, we first give a brief description of the CMB polarization as follows: A photon scattered by an electron is polarized perpendicular to the incident direction. When the incident photons are isotropic or have only a dipole distribution, there is no net polarization of the scattered photons. On the other hand, if the incident photons are perpendicular to each other and have different intensities, the scattered photons will have a net linear polarization. In addition, photons are polarized by the perturbed gravitational potential, e.g. weak lensing effects. The polarization of photons with positive parity is called the "E-mode", and the polarization with negative parity is called the "B-mode". Therefore, there are three observable modes: the T -mode; the E -mode and the B -mode. From these, one can generate correlations leading to three power spectra denoted: TT , EE , and BB . There are also three cross-correlation spectra: TE , TB , and EB . The only nonzero spectra, however, are the TT , EE , BB , and TE modes due to parity considerations. Also, the modes can have up to three kinds of fluctuations: scalar, vector and tensor.

Figure 2 illustrates that a PMF produces the largest temperature fluctuations and polarization anisotropies of the CMB for higher multipole moments ℓ . The energy density of the PMF is proportional to the fourth power of the scale factor a^{-4} just like the photon energy density. On the other hand, the field strength of the PMF scales with the plasma density ρ_{p0} as

$$B_\lambda(k, a) = B_\lambda(k) * (\rho_{p0} + \delta\rho_p) \quad (14)$$

where $\delta\rho_p$ is a first order perturbation in the plasma density. If the field strength of the PMF is less than the order of 10 nG, the energy density of the PMF is less than or equal to the perturbations in the energy density of the CMB photons. Thus, the second term of Eq.(14) is a second order perturbation and negligible in the linearized theory. Therefore, we can ignore the effect of the time evolution of the plasma density fluctuations (e.g. Silk damping [63]) on the PMF in the linear theory. As a result, the effects of a PMF on the temperature fluctuations and polarization anisotropies of the CMB tend to be large even for scales smaller than the Silk damping scale.

For the vector mode, the CMB polarization due to a PMF is largest for higher multipole moments, ℓ , while the tensor mode of the PMF diminishes for large multipoles [cf. Fig.2] [64, 4, 15, 23]. The reason for this is that the gravity waves from the PMF can be negligibly small after horizon crossing. They are small because, once inside the horizon, the homogeneous solution for the gravity waves begins to oscillate and decay rapidly. [65, 66, 67, 68]. As a result, the effect of gravity waves from the PMF only occurs on scales larger than the horizon at the epoch of the generation of the CMB ($z \sim 1000$).

There are several degeneracies between the PMF and other physical processes in the early universe. Panel (b) on Figures 2 and 3 shows the BB mode of the CMB polarization from the primary fluctuations, gravitational lensing, and the PMF. We can see that the total BB mode spectrum is dominated by the PMF for $B_\lambda \gtrsim 2.0$ nG and $\ell \gtrsim 200$. We must, however, consider the degeneracy between the PMF and lensing effects on such small angular scales. This is because the BB mode is converted from the EE mode by a gravitational lensing effect on these angular scales [68]. However, the source of the spectrum from the gravitational lensing signal is the EE -mode of the CMB polarization of the primary scalar fluctuations. Fortunately, however, this spectrum can be subtracted directly because the EE -mode polarization of the primary scalar fluctuations have been determined independently.

Since the Sunyaev-Zel'dovich effect is one of the main foreground sources for higher ℓ [69], we must also consider the degeneracy between the PMF and the Sunyaev-Zel'dovich effect on the temperature fluctuations of the CMB. Nevertheless, the effects of a PMF on the CMB background are independent of frequency and the Sunyaev-Zel'dovich effect on the CMB as a foreground depends upon the frequency. Therefore, it should be possible to distinguish the effects of a PMF from such foreground effects by making observations at different frequencies.

The qualitative features of the constrained parameters of the PMF from only the CMB observations are easy to understand. Table 1 shows the constraint on the PMF parameters from the combined CMB observations of WMAP, ACBAR and CBI using Markov Chain Monte Carlo (MCMC) methods [70]. We find that there is no obvious degeneracy between the PMF and cosmological parameters. The reason for this is that the effects of a PMF dominate for $\ell > 1000$, while the other cosmological parameters are constrained by the WMAP power spectrum obtained for $\ell < 1000$.

On the other hand, from Fig. 4 one can see that there is a strong degeneracy between the PMF amplitude B_λ and the power law spectral index n_B .

There are two main reasons for this. For one, the effect of a PMF on the CMB is to produce a peak in the range of $\ell \geq 1500$. Unfortunately, however, observations are not yet precise enough in this multipole range to constrain the PMF parameters. This is especially true for the BB mode for higher ℓ where we do not yet have observations of the BB mode with sufficiently small error. The second reason is simply that the PMF parameters themselves induce similar effects on the amplitude of the CMB power spectrum [12, 15].

3.3. Constraints from LSS

There are strong constraints on parameters of the PMF from the observed limits on the σ_8 parameter [see [28] for details]. This parameter is determined from a weighted integral of the matter power spectrum [71] and corresponds to the root-mean-square of the matter density fluctuations in a comoving sphere of radius $8h^{-1}$ Mpc.

Figure. 5 shows that the density fluctuations of matter are more strongly affected by a PMF for wavenumbers $k/h > 0.1 \text{ Mpc}^{-1}$ [28]. As mentioned in Sec. 3.2, the time evolution of the PMF energy density does not depend on the time evolution of the plasma density fluctuations (e.g. Silk damping) in the linear theory. Therefore, the PMF can survive as a source of temperature fluctuations and polarization anisotropies of the CMB on scales well below the photon diffusion length.

The baryons influence the cold dark matter (CDM) through gravity. This effect is very small before the epoch of photon last scattering ($z \simeq 1000$) because the baryon density oscillates with the photons and their gravitational effect on the CDM becomes very small. However, after the baryons decouple from the photons, the baryon density begins to affect the density of the CDM through gravitational interactions [72]. Also, the baryons are influenced by any PMF present in the early universe. Thus, a PMF can indirectly affect the CDM evolution. Nevertheless, it is reasonable to assume that the energy density of the PMF is independent of the matter density fluctuations. In this case, the PMF merely increases the matter power spectrum independently of whether the pressure or tension dominate the PMF [28].

As discussed in Sec. 3.2, there is the strong degeneracy between the PMF amplitude B_λ and the power law spectral index n_B . Thus, one needs a good Bayesian prior constraint to effectively decouple these two parameters characterizing the PMF. In this regards one is aided by the observed constraints

on the σ_8 parameter. The parameter σ_8 is constrained by observational data on linear cosmological scales [73, 74, 57, 56] to lie in the range $0.7 < \sigma_8 < 0.9$.

Fortunately, the recent CMB observations have determined cosmological parameters based upon the power spectrum obtained on larger scales ($\ell < 1000$) [54, 52, 53]. The effects of the PMF are mainly on smaller scales ($\ell > 1000$) [12, 28, 15]. Therefore, one expects that there is only a small degeneracy between the PMF parameters and the other cosmological parameters. Hence, if one wishes to understand the qualitative nature of how the PMF parameters are constrained by observations of LSS, one is justified in fixing the other cosmological parameters at their best fit values from the WMAP analysis.

In Fig. 6 we show the optimum PMF parameters n_B and B_λ for various constant values of σ_8 . The power spectrum of the PMF $P_{PMF}(k)$ scales [15] as:

$$P_{PMF}(k) \propto k^{2n_B+3}. \quad (15)$$

Therefore, for $n_B < -1.5$, the effect of a PMF on the density fluctuations on small scales decreases with smaller values for n_B . In the case that n_B is near -3.0 , the matter power spectrum including the PMF effects diminishes for smaller scales. Hence, larger amplitudes of B_λ are allowed. However, for $n_B > -1.5$ the PMF power spectrum is proportional to the cut-off scale as $k_C^{2n_B+3}$ [15] where k_C is proportional to $B_\lambda^{-1/(n_B+5)}$ [75, 76, 77, 15]. Substituting these relations into Eqs.(15)-(17) in Ref. [15], an expression for the relation between the power spectrum of the PMF and the magnetic strength can be deduced,

$$P(k)_{PMF} \propto B_\lambda^{[14/(n_B+5)]}. \quad (16)$$

When $B_\lambda \ll 1\text{nG}$, the matter power spectrum including the effect of the PMF for $n_B > -1.5$ becomes larger for larger n_B . In this case a large strength of B_λ is not allowed for larger n_B .

If the PMF has no correlation with the primary density fluctuations, the effect of a PMF is to increase the matter power spectrum independently of whether the PMF pressure or tension dominates [15]. As noted above, recent cosmological observations of LSS imply $\sigma_8 > 1$ can be excluded. Therefore, we can exclude field strengths of $B_\lambda \gtrsim 1\text{ nG}$ if $n_B > -0.9$ (Fig. 6) and $B_\lambda \gtrsim 0.1\text{ nG}$ if $n_B > 0.2$. When the PMF evolves to the observed magnetic field in clusters of galaxies, we can expect that the PMF amplitude is $B_\lambda \gtrsim 1\text{ nG}$. In this case from Fig.6 we can exclude spectral indices of $n_B > -0.9$.

3.4. Concordance MCMC analysis

Constraints on parameters of the PMF have been deduced by our group [23] and other groups [61, 62]. These constraints are based upon fits to the CMB and LSS observational data in the context of a flat Lambda CDM cosmology. This cosmology is characterized by six standard parameters i.e. $\{\Omega_b h^2, \Omega_c h^2, \tau_C, n_s, \log(10^{10} A_s), A_t/A_s, |B_\lambda|, n_B\}$, where $\Omega_b h^2$ and $\Omega_c h^2$ are the baryon and CDM densities in units of the critical density, h denotes the present Hubble parameter in units of $100 \text{ km s}^{-1} \text{ Mpc}^{-1}$, τ_C is the optical depth for Compton scattering, n_s is the spectral index of the primordial scalar fluctuations, A_s is the scalar amplitude of the primordial scalar fluctuations and A_t is the scalar amplitude of the primordial tensor fluctuations. We define the tensor index for the primordial tensor fluctuations as $n_t = -(A_s/A_t)/8$. For these standard parameters one can adopt the Bayesian priors used in the previous WMAP analysis [54, 52, 53, 78] without a PMF. To the standard cosmological parameters, one then adds the two PMF parameters: the spectral index n_B ; and the average magnetic field strength on a comoving scale B_λ .

Using a MCMC method with cosmological observations (e.g. the CMB and/or LSS) the standard cosmological parameters and the PMF parameters have been constrained [23]. The results of this analysis are summarized in Table 1. However, we note that an inherent flaw in the MCMC approach is a sparse sampling of points near the boundary. Consequently, this method tends to assign low probability near a boundary. This is the reason that the PMF power law index n_B seems to be constrained even in the limit of $B_\lambda \rightarrow 0$. In reality, of course, the spectral index n_B is not constrained for $B_\lambda = 0$. However, this shortcoming does not negate the result that a finite magnetic field and spectral index give a genuine minimum likelihood in the goodness of fit. In the best fit including the PMF parameters, the minimum total χ^2 is improved from 2803.4 to 2800.2 corresponding to an improvement of the reduced χ^2 from 1.033 to 1.031. This slight improvement implies that the existence of the PMF is still only of marginal significance.

Figures 7 and 8 show the 68% and 95% C.L. probability contours in the planes of each standard cosmological parameter versus field strength of the PMF or power law index. Also shown are the probability distributions. The bottom panels of Fig. 7 and Fig. 8 show the probability distributions for $|B_\lambda|$ and n_B . Of particular note for this MCMC analysis is that a parameter set of $|B_\lambda| = 0.85 \pm 1.25 \text{ nG}$ and $n_B = -2.37_{-0.73}^{+0.88}$ maximizes the likelihood. These values of the PMF parameters are consistent with no magnetic field,

and thus provide only imply upper limits. Nevertheless, they suggest that it may be possible to detect a finite PMF with forthcoming data (particularly for large CMB multipoles).

These figures also confirm that there is no degeneracy between the standard cosmological parameters and the PMF. We can see this from Table 1 in which it is apparent that the standard cosmological parameters do not significantly differ from those deduced directly from the WMAP data without the introduction of a PMF. As mentioned above, the reason for this is simple. The standard cosmological parameters are mainly derived from the observed CMB for low multipoles $\ell < 1000$ (up to the 2nd acoustic peak), while the PMF is most important for $\ell > 1000$. Thus, the PMF effect on the CMB power spectrum is nearly independent of the standard cosmological parameters.

The tensor to scalar ratio A_t/A_s in our analysis is defined as the primary tensor amplitude without the PMF. When we compare our tensor amplitude with the cosmological observations by the MCMC method, we combine the tensor amplitude from the PMF $A_{t[\text{PMF}]}$ and A_t . Therefore the upper limit to the tensor to scalar ratio A_t/A_s in our analysis is less than the A_t/A_s ratio constrained from the WMAP analysis without a PMF ($A_t/A_s < 0.43$, 95% CL). Actually, the upper limit of $(A_t + A_{t[\text{PMF}]})/A_s$ constrained by our analysis including a PMF is consistent with the previous constraints. In addition, the effects of a PMF on the matter power spectrum and the CMB temperature fluctuations and polarization anisotropies dominate for smaller scale e.g. $\ell > 1000$, while the PMF contribution to the CMB for larger scales is negligible compared to the primary CMB fluctuations of the scalar and tensor modes [16, 79]. Therefore, the tensor to scalar ratio is not affected by the presence of a PMF.

Figure 8 shows the deduced probability distributions and the 1σ and 2σ (68% and 95% C.L.) probability contours for the derived parameters, σ_8 , H_0 , z_{reion} , and Age, where H_0 is the Hubble parameter in units of $\text{km s}^{-1} \text{Mpc}^{-1}$, z_{reion} is the red shift at which re-ionization occurs, and Age is the presently observed age of the universe in Gyr. In Fig. 8, one can see by the slight bend in the contours that there is a weak degeneracy between the PMF parameters and σ_8 . The reason for this is that the matter power spectrum for smaller scale determines both σ_8 and the PMF parameters.

Table 1 summarizes the constrained PMF parameters together with the standard and derived cosmological parameters. The best constraints on the

PMF determined yet to date determined in our analyses are [23]:

$$|B_\lambda| < \mathbf{2.10} \text{ nG (68\%CL)} , < \mathbf{2.98} \text{ nG (95\%CL)} \quad (17)$$

on a present scale of 1 Mpc, and

$$n_B < \mathbf{-1.19} \text{ (68\%CL)} , < \mathbf{-0.25} \text{ (95\%CL)}. \quad (18)$$

This result differs only slightly from the constraints obtained in [80, 62] based upon different observations.

Adopting these PMF constraints and the BBN GWB constraint discussed above [49], a re-examination of the three main PMF generation scenarios [33, 34, 35, 36] is motivated by the present results. Figure 9 summarizes the contours of $|B_\lambda|$ and n_B at the 1 and 2 σ C.L. along with the associated GWB constraints for the three generation epochs.

The region bounded by the yellow area corresponds to the 2 σ C.L. on PMF parameters. The upper limit of the produced PMF from big-bang nucleosynthesis, the electroweak transition, and the inflation epoch are shown by the green, blue, red lines, respectively. However, as mentioned above, there is not yet a lower limit for the PMF parameters, B_λ and n_B at the 2 σ C.L. On the other hand, considering the region bounded by the σ C.L. red orange area, one can find both upper and lower limits to the PMF strength. Figure. 9 shows that the allowed or excluded regions based upon these multiple constraints depends upon when the PMF was generated as follows:²

At the 2 σ C.L. there are only upper limits to $|B_\lambda|$ and no limits on n_B . These are:

I. Inflation:

$$|B_\lambda| \lesssim 2.90 \text{ nG} \quad (19)$$

II. Electroweak transition:

$$|B_\lambda| \lesssim 3.08 \text{ nG} \quad (20)$$

²The 1 σ and 2 σ regions on the two parameter plane like Fig.9 do not directly indicate constrained values of the parameters at 1 σ and 2 σ as given in Table 1

III. BBN:

$$|B_\lambda| \lesssim 3.10 \text{ nG} \tag{21}$$

At the 1σ C.L. there are both upper lower limits to $|B_\lambda|$ and n_B . These are:

I. Inflation:

$$\begin{aligned} 0.292 \text{ nG} &\lesssim |B_\lambda| \lesssim 2.33 \text{ nG} \\ -2.97 &\lesssim n_B \lesssim -2.66 \end{aligned}$$

II. Electroweak transition:

$$\begin{aligned} 0.117 \text{ nG} &\lesssim |B_\lambda| \lesssim 2.46 \text{ nG} \\ -2.97 &\lesssim n_B \lesssim -2.11 \end{aligned}$$

III. BBN:

$$\begin{aligned} 0.117 \text{ nG} &\lesssim |B_\lambda| \lesssim 2.48 \text{ nG} \\ -2.97 &\lesssim n_B \lesssim -2.03 \end{aligned}$$

If the PMF were generated at an even earlier epoch, it is clear that upper limits on both $|B_\lambda|$ and n_B would be more stringent. These limits are the strongest constraints on the PMF that have yet been determined. However, one should keep in mind that the evolution and/or the generation of the magnetic field on cosmological scales during the formation of LSS is not well understood. Therefore, if there are other effective physical scenarios for the generation and/or evolution of the PMF after the epoch of the photon last scattering, our lower limits to the PMF parameters will change. To accurately constrain the PMF parameters, one should study the PMF not only before but also after the epoch of photon last scattering.

4. Discussion and Future Challenges

The generation and/or the evolution of the PMF along with its physical behavior in the early universe have been studied by many researchers [see [29] for a recent review]. In this section we review several relevant topics and their implications for different PMF strengths. We also discuss future prospects for studying the role of the PMF in cosmology, astrophysics and astronomy.

Cosmological Parameters

Parameter	mean	best fit
$\Omega_b h^2$	0.02320 ± 0.00059	0.02295
$\Omega_c h^2$	0.1094 ± 0.0046	0.1093
τ_C	0.087 ± 0.017	0.082
n_s	0.977 ± 0.016	0.970
$\ln(10^{10} A_s)$	3.07 ± 0.036	3.06
A_t/A_s	$< 0.170(68\%CL), < 0.271(95\%CL)$	0.0088
$ B_\lambda (\text{nG})$	$< \mathbf{2.10}(68\%CL), < \mathbf{2.98}(95\%CL)$	0.85
n_B	$< \mathbf{-1.19}(68\%CL), < \mathbf{-0.25}(95\%CL)$	-2.37
σ_8	$0.812^{+0.028}_{-0.033}$	0.794
H_0	73.3 ± 2.2	72.8
z_{reion}	10.9 ± 1.4	10.5
Age(Gyr)	13.57 ± 0.12	13.62

Table 1: PMF parameters and Λ CDM model parameters and 68% confidence intervals (A_t/A_s is a 95% CL) from a fit to the seven year WMAP [81] + ACBAR [82] + CBI [83] +Boomerang [84] + 2dFDR [73] data.

4.1. The BB mode from the PMF

As mentioned above, a PMF affects not only the temperature fluctuations, but also the polarization anisotropies of the CMB. Although fits have been based upon all available temperature and polarization data of the CMB, it turns out that the TT and BB modes are the most important for constraining the parameters of the PMF. Figs. 10 (the TT-mode) and 11 (the BB-mode) show a comparison of the observations of the CMB with the computed best-fit total power spectrum. Figure 10 shows the best fit and allowed regions including both the Sunyaev Zel’dovich (SZ) effect (scattering from re-ionized electrons) at the K(22.8GHz) band (upper curves) and without the SZ effect (lower curves). Including the SZ effect only slightly diminishes the best fit magnitude of the PMF.

Figure 10 exhibits the best-fit and allowed regions (or curve) both including the SZ effect at 22.8GHz (upper curves) and without the SZ effect (lower curves). Since the temperature fluctuations of the CMB from recent observations have become more accurate than the data shown in Fig. 10, these observations give a strong prior range for constraining parameters of the PMF. However, as discussed above, we cannot determine the parameters of the PMF by the TT mode alone because there is a strong degeneracy

between the field strength and the power law index of the PMF. On the other hand, the effects of a PMF on the BB-mode of the CMB has a feature for $\ell > 200$ as shown in Fig. 11. This is due to the vector source from the PMF[12, 15]. Thus, if accurate observations of the BB mode could be obtained in the future, one expects that the parameters of the PMF could be constrained without the uncertainty due degeneracy between the field strength and the power law index.

4.2. *PMF and GWB*

Several groups [49, 59] have studied the GWB induced by a PMF. From such studies, one expects that there is a degeneracy between the GWB from inflation and that generated by a PMF. Indeed, if the PMF is generated during the inflation epoch this degeneracy would become stronger. This is particularly true since the power spectrum of an inflation-generated PMF is expected to be nearly scale-invariant. Therefore, even if the GWB is observed in the future, it will still be difficult to constrain the parameters of the PMF from these observations alone(See Fig.12).

There is, however, a difference. The GWB from inflation mainly affects the tensor BB mode of the CMB, while a PMF affects both the vector and tensor polarizations of the BB mode of the CMB [15, 23]. Thus, the BB mode exhibits different features in the GWB from a PMF or an inflation origin. Since both a PMF and inflation dominate the tensor source on the same scales of the BB mode, there is a strong degeneracy between the BB mode of tensor type polarizations from the PMF and inflation. However, the PMF also has a vector type polarization as a source of the BB mode of the CMB and this mode is most important on smaller angular scale e.g. $\ell > 200$, while both tensor sources of the PMF and inflation dominate the BB mode on larger angular scales e.g. $\ell > 200$. Therefore, if one could simultaneously obtain observations of the GWB and the tensor and vector BB modes of the CMB, this degeneracy may be resolved.

4.3. *Constraint on the neutrino mass in the presence of a PMF*

The presence of a PMF can alter the particle constraints deduced from the CMB. If the velocities of finite-mass neutrinos are large enough, the growth of density fluctuations is impeded on the free-streaming-scale of the neutrinos [85]. Hence, the matter density field in the early universe can be affected by a finite neutrino mass [86]. The inferred cosmological constraints on the mass of the neutrino are of considerable interest. The sum of the neutrino masses

is constrained to be $\sum_{\nu} m_{\nu} \leq 0.1 - 1$ eV by a combination of cosmological observations [87, 88, 89, 58] and the results of tritium beta-decay endpoint experiments [90]. On the other hand, as explained Sec. 3.3, a PMF affects the matter density fields in the early universe and the parameters of the PMF correlate with σ_8 . Therefore, there is a possible degeneracy between the parameters of the PMF and the mass of the neutrino. This degeneracy relaxes the cosmological constraint on the sum of the neutrino masses.

In Fig. 13 we show the constraints on the sum of the neutrino masses $\sum_{\nu} m_{\nu}$ and B_{λ} for various fixed values of n_B and ranges of σ_8 . The expected field strength of the PMF from cosmological observations is $B_{\lambda} < 2.0\text{nG}(1\sigma)$ and $< 3.0\text{nG}(2\sigma)$, while σ_8 is constrained to be in the range $0.75 < \sigma_8 < 0.85$. For this range of σ_8 , if we do not consider the effect of a PMF on the matter density field, the constrained sum of the neutrino masses is less than 0.11 eV. On the other hand when a PMF is introduced, the upper limit on the sum of the neutrino masses from Fig. 13, increases to $\sum_{N_{\nu}} m_{\nu} < 0.24$ eV for $n_B = -1.5$ and $< 0.6\text{eV}$ for $n_B = -2.5$ and $N_{\nu} = 3$. Since the effect of a PMF cancels the effect of neutrinos on the density fluctuations, the constrained mass of the neutrinos when a PMF is present is larger than that deduced without considering a PMF.

However, σ_8 depends upon the cosmological model employed and it has some degeneracy with $\Omega_m = \Omega_b + \Omega_{\text{CDM}}$, n_s , and A_s , even if these primary parameters are well constrained by the CMB data, e.g. WMAP[58]. Furthermore, the neutrino mass has a degeneracy with Ω_m [91]. Thus, one should ultimately consider the simultaneous degeneracy between the standard cosmological parameters, the mass of neutrinos and the PMF. With high precision observations on small angular scales, it may be possible in the near future to obtain not only upper but also lower limits to the mass of the neutrinos from cosmology and astrophysics in the presence of the PMF.

4.4. *Non-Gaussianity from a PMF*

If we assume that the inflation mode is simple, then the primordial fluctuations will be Gaussian. A measurement of non-Gaussianity in the primordial fluctuations could thus provide important evidence for new physics beyond that of simple inflation[92]. Recently, however, several authors have shown that a PMF can cause non-Gaussianity[93, 94, 95, 96, 97].

We can constrain the non-Gaussianity by auto- and cross correlated bispectra from the intensity fluctuations of the CMB. On the other hand, the bispectra from the CMB are also affected by a PMF. Therefore, one expects

that the effects of a PMF and inflation on the non-Gaussianity of the CMB will have a degeneracy. Hence, even if one could obtain accurate observations of the non-Gaussianity of the CMB, one would not be able to analyze the inflation model without information on the effects from the PMF. To solve this degeneracy and truly understand the inflation model, one should consider the constraints on PMF effects by various observations, e.g. BBN, the GWB, LSS, and the CMB.

4.5. 21 cm line and a PMF

The 21 cm line is emitted by a transition of the neutral hydrogen atom between the two different energy levels of its 1s ground state. Since hydrogen is the most abundant element in the Universe (75 % of normal matter by mass and 90 % by number), it is important to survey the 21 cm line for researching the "Dark Age"³. If observations of the 21 cm are successful, one should be able to obtain a precise matter power spectrum after recombination and the re-ionization of the Universe[98].

As mentioned above, a PMF affects structure formation in the early Universe. Furthermore, a PMF of strength ~ 1 nG reheats the intergalactic medium (IGM) including hydrogen up to several thousand K through ambipolar diffusion[19]. Therefore, the 21 cm line is indirectly affected by a PMF. The Square Kilometer Array (SKA)⁴ is planning a most promising future project for observing the cosmological 21 cm line. One should consider the effects of a PMF on the 21 cm line to obtain an accurate physical interpretation from the results of observations like that of the SKA.

³Considering the cosmological redshift, the 21 line is observed in a frequency range from about 200MHz to 9 MHz.

⁴the detected frequency range of the SKA project will be from 70 MHz to 10GHz.

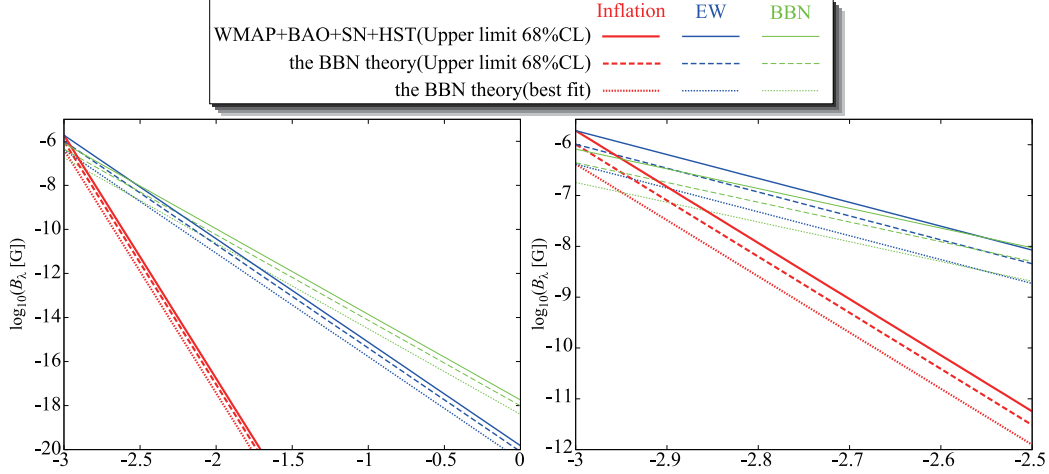


Figure 1: Constrained parameter plane of the PMF field strength B_λ vs. the power spectral index n_B by the BBN. The thin (green), middle (blue), and bold (red) lines show upper limits on the produced PMF during the epoch of BBN, the electroweak transition, and the inflation epoch, respectively. (For interpretation of the references to colour in this figure legend, the reader is referred to the web version of this article.)

Acknowledgments

This work has been supported in part by Grants-in-Aid for Scientific Research (20105004, 20244035, 20169444, 21740177 and 22012004) of the Ministry of Education, Culture, Sports, Science and Technology of Japan. This work is also supported by the JSPS Core-to-Core Program, International Research Network for Exotic Femto Systems (EFES) and Heiwa Nakajima Foundation. Work at UND supported in part by the US Department of Energy under research grant DE-FG02-95-ER40934.

References

- [1] K. Subramanian, J. D. Barrow, Microwave background signals from tangled magnetic fields, *Phys. Rev. Lett.* 81 (1998) 3575–3578.
- [2] A. Mack, T. Kahniashvili, A. Kosowsky, Vector and tensor microwave background signatures of a primordial stochastic magnetic field, *Phys. Rev. D* 65 (2002) 123004.
- [3] K. Subramanian, J. D. Barrow, Small-scale microwave background

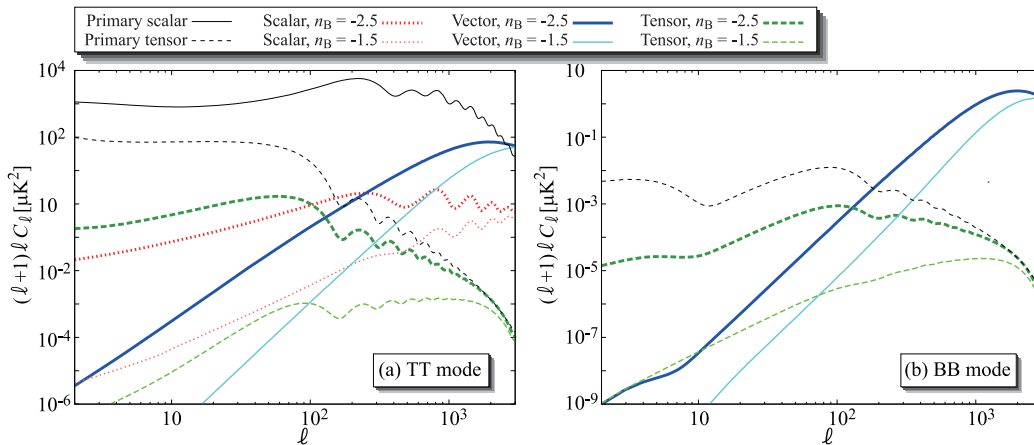


Figure 2: Temperature fluctuations [TT mode on Panel (a)] and polarization anisotropies [BB mode on Panel (a)] of the CMB from the primary energy density and the PMF. We plot models with $B_\lambda = 3.0$ nG and $n_B = -1.5$ and -2.5 as labeled. The scalar to tensor ratio for this plot is taken to be 0.2 for the primary tensor contribution.

anisotropies due to tangled primordial magnetic fields, Mon. Not. Roy. Astron. Soc. 335 (2002) L57.

- [4] A. Lewis, Cmb anisotropies from primordial inhomogeneous magnetic fields, Phys. Rev. D 70 (2004) 043011.
- [5] D. G. Yamazaki, K. Ichiki, T. Kajino, Constraining primordial magnetic field from cmb anisotropies at higher multipoles, Astrophys. J. 625 (2005) L1–L4.
- [6] T. Kahniashvili, B. Ratra, Effects of cosmological magnetic helicity on the cosmic microwave background, Phys. Rev. D 71 (2005) 103006.
- [7] A. Challinor, Cosmic microwave background polarization analysis, Lect. Notes Phys. 653 (2004) 71–104.
- [8] A. D. Dolgov, Cosmological magnetic fields and cmb polarization [arXiv:astro-ph/0503447](https://arxiv.org/abs/astro-ph/0503447).
- [9] R. Gopal, S. K. Sethi, Tangled magnetic fields and cmb signal from reionization epoch, Phys. Rev. D 72 (2005) 103003.
- [10] D. G. Yamazaki, K. Ichiki, T. Kajino, Primordial magnetic field at the photon last scattering surface, Nuclear Physics A 758 (2005) 791–794.

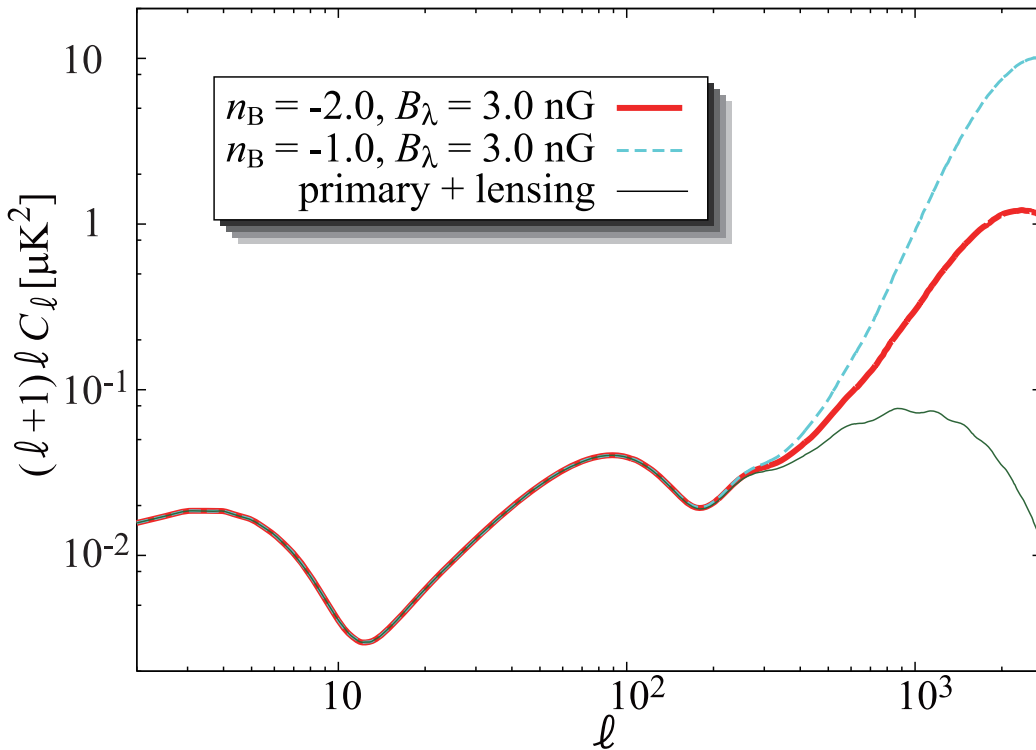


Figure 3: BB mode from the PMF. The bold (red) and dashed (azure) curves show results for $(B_\lambda, n_B) = (3.0\text{nG}, -2.0)$ and $(B_\lambda, n_B) = (3.0\text{nG}, -1.0)$. The thin (green) curve shows the primary tensor mode power spectrum (without the PMF) with weak lensing effects included. (For interpretation of the references to colour in this figure legend, the reader is referred to the web version of this article.)

- [11] T. Kahniashvili, B. Ratra, CMB anisotropies due to cosmological magnetosonic waves, *Phys. Rev. D* 75 (2007) 023002.
- [12] D. G. Yamazaki, K. Ichiki, T. Kajino, G. J. Mathews, Constraints on the evolution of the primordial magnetic field from the small-scale cosmic microwave background angular anisotropy, *Astrophys. J.* 646 (2006) 719–729.
- [13] D. G. Yamazaki, K. Ichiki, T. Kajino, G. J. Mathews, Primordial magnetic field constrained from cmb anisotropies, and its generation and evolution before, during and after the bbn, *PoS(NIC-IX)*. (2006) 194.

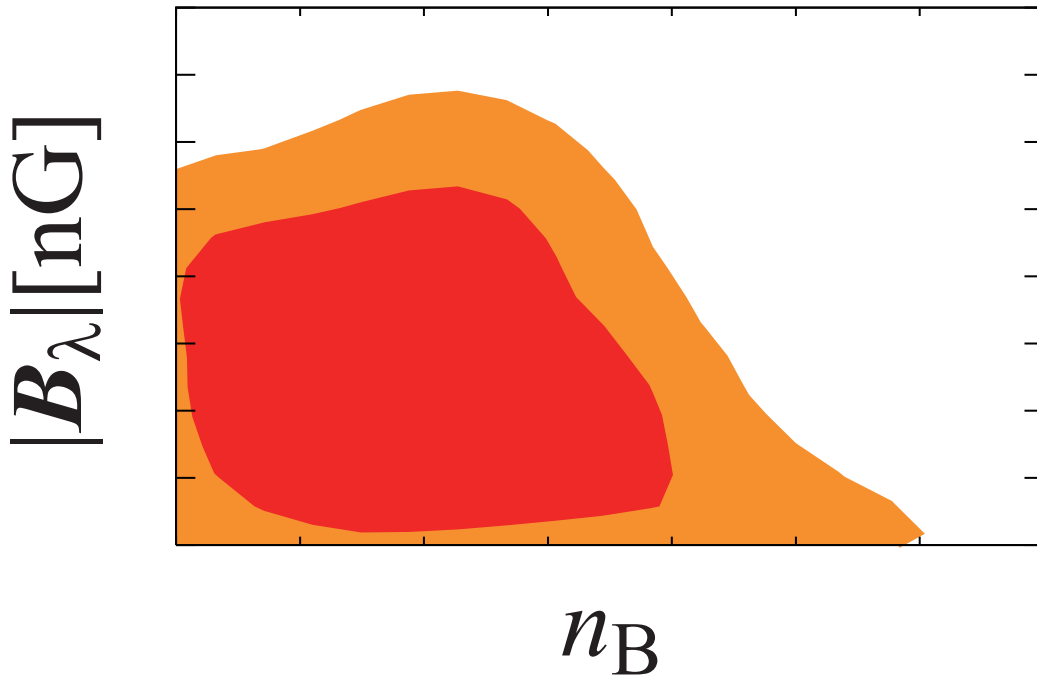


Figure 4: Probability contour plane of n_B vs. B_λ from an MCMC analysis of the CMB and LSS observations. Deep (red) and pale (orange) colour contours show the 1σ (68%) and 2σ (95%) confidence limits. (For interpretation of the references to colour in this figure legend, the reader is referred to the web version of this article.)

- [14] M. Giovannini, Tight coupling expansion and fully inhomogeneous magnetic fields, *Phys. Rev. D* 74 (2006) 063002.
- [15] D. G. Yamazaki, K. Ichiki, T. Kajino, G. J. Mathews, Effects of a primordial magnetic field on low and high multipoles of the cosmic microwave background, *Phys. Rev. D* 77 (2008) 043005.
- [16] D. Paoletti, F. Finelli, F. Paci, The full contribution of a stochastic background of magnetic fields to CMB anisotropies, *Mon. Not. Roy. Astron. Soc.* 396 (2009) 523–534.
- [17] D. G. Yamazaki, K. Ichiki, T. Kajino, G. J. Mathews, Constraints on the primordial magnetic field from σ_8 , *Phys. Rev. D* 78 (2008) 123001.
- [18] D. G. Yamazaki, K. Ichiki, T. Kajino, G. J. Mathews, A Strong Constraint on the Neutrino Mass from the Formation of Large Scale Struc-

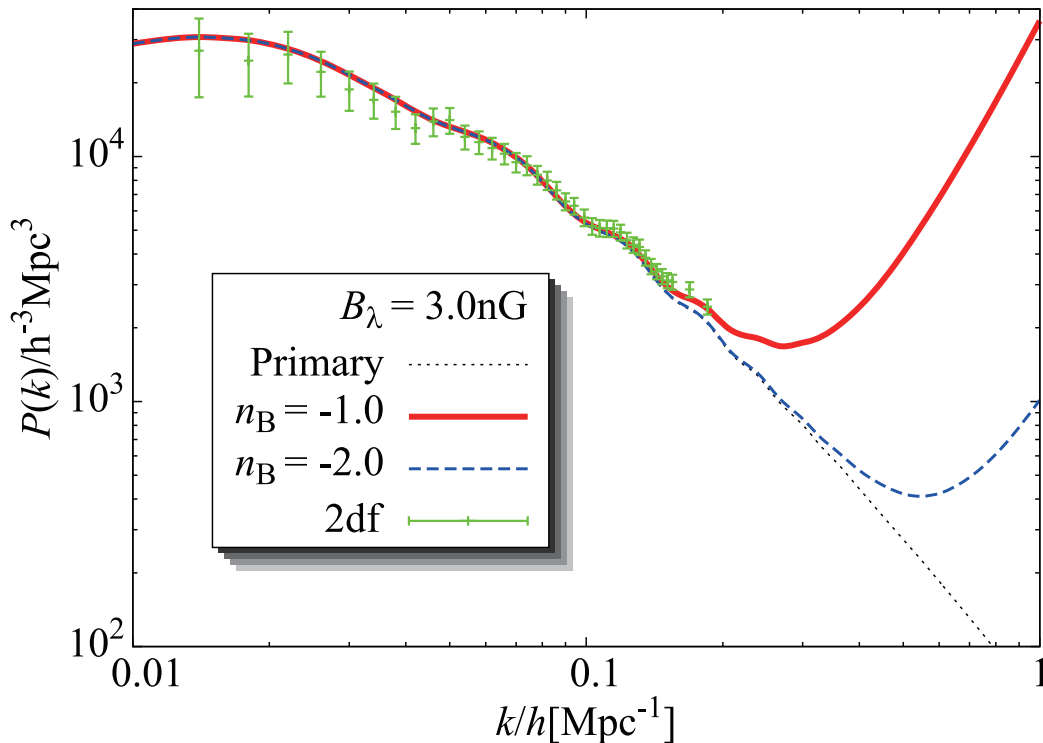


Figure 5: Matter power spectra of the primary CMB, the observational result, and the PMF for $B_\lambda = 3.0$ nG. Bold (red) and dashed (blue) curves are for $n_B = -2.0$ and -1.0 . The dotted (black) curve is the primary CMB power spectrum. The dots with error bars are from an analysis of the 2dF data[73]. (For interpretation of the references to colour in this figure legend, the reader is referred to the web version of this article.)

ture in the Presence of the Primordial Magnetic Field, PoS(NIC-X). (2008) 239.

- [19] S. K. Sethi, B. B. Nath, K. Subramanian, Primordial magnetic fields and formation of molecular hydrogen, Mon. Not. Roy. Astron. Soc. 387 (2008) 1589–1596.
- [20] K. Kojima, K. Ichiki, D. G. Yamazaki, T. Kajino, G. J. Mathews, Neutrino mass effects on vector and tensor CMB anisotropies in the presence of a primordial magnetic field, Phys. Rev. D78 (2008) 045010.
- [21] T. Kahniashvili, G. Lavrelashvili, B. Ratra, CMB temperature

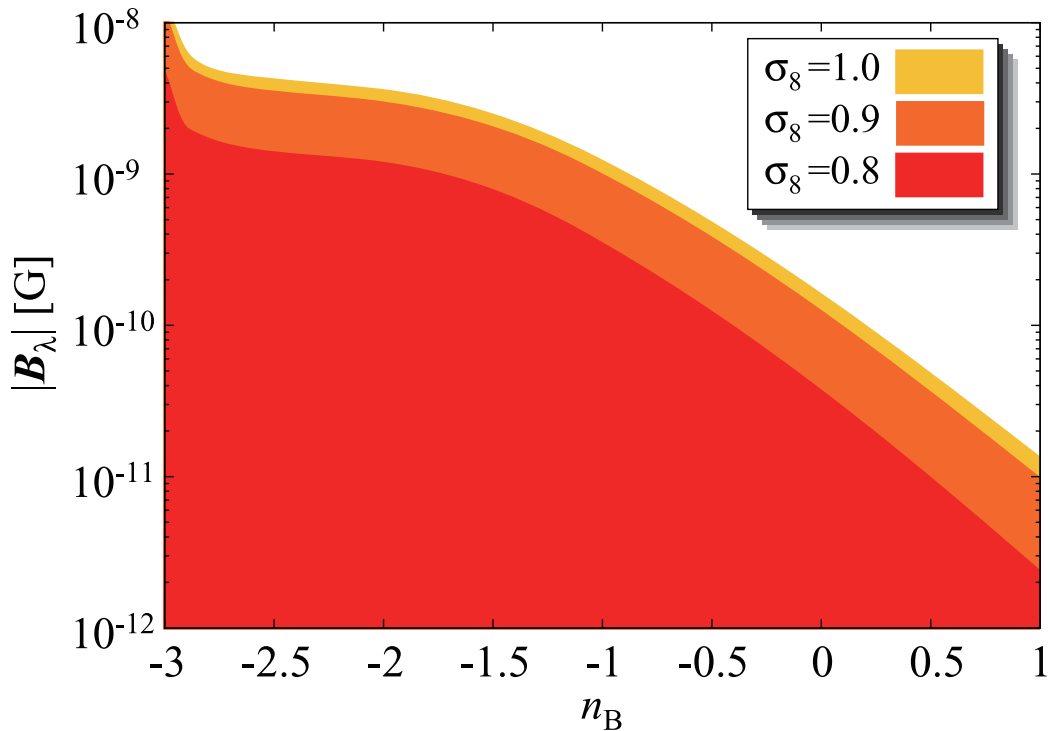


Figure 6: Constrained B_λ vs. n_B plane by the σ_8 . The deep (red), middle (orange) and pale (yellow) areas are for $\sigma_8 \leq 0.8, 0.9$ and 1.0 , respectively. (For interpretation of the references to colour in this figure legend, the reader is referred to the web version of this article.)

anisotropy from broken spatial isotropy due to a homogeneous cosmological magnetic field, Phys. Rev. D78 (2008) 063012.

- [22] M. Giovannini, K. E. Kunze, Faraday rotation, stochastic magnetic fields and CMB maps, Phys. Rev. D78 (2008) 023010. [arXiv:0804.3380](https://arxiv.org/abs/0804.3380), doi:10.1103/PhysRevD.78.023010.
- [23] D. G. Yamazaki, K. Ichiki, T. Kajino, G. J. Mathews, New constraints on the primordial magnetic field, Phys. Rev. D 81 (2010) 023008.
- [24] D. G. Yamazaki, K. Ichiki, T. Kajino, G. J. Mathews, Constraints on the neutrino mass and the primordial magnetic field from the matter density fluctuation parameter σ_8 , Phys. Rev. D 81 (2010) 103519.
- [25] D. G. Yamazaki, K. Ichiki, T. Kajino, G. J. Mathews, Primordial Mag-

- netic Field Effects on the CMB and Large-Scale Structure, *Advances in Astronomy* 2010 (2010) 586590. doi:10.1155/2010/586590.
- [26] S. K. Sethi, Large Scale Magnetic Fields: Galaxy Two-Point correlation function, *Mon. Not. Roy. Astron. Soc.* 342 (2003) 962.
 - [27] S. K. Sethi, K. Subramanian, Primordial Magnetic Fields in the Post-recombination Era and Early Reionization, *Mon. Not. Roy. Astron. Soc.* 356 (2005) 778–788.
 - [28] D. G. Yamazaki, K. Ichiki, K. I. Umezu, H. Hanayama, Effect of primordial magnetic field on seeds for large scale structure, *Phys. Rev. D* 74 (2006) 123518.
 - [29] A. Kandus, K. E. Kunze, C. G. Tsagas, Primordial magnetogenesis, *Physics Reports*, 505 (2011) 1–58.
 - [30] M. S. Turner, L. M. Widrow, Inflation produced, large scale magnetic fields, *Phys. Rev. D* 37 (1988) 2743.
 - [31] B. Ratra, Cosmological 'seed' magnetic field from inflation, *Astrophys. J.* 391 (1992) L1–L4.
 - [32] K. Bamba, J. Yokoyama, Large-scale magnetic fields from dilaton inflation in noncommutative spacetime, *Phys. Rev. D* 70 (2004) 083508.
 - [33] T. Vachaspati, Magnetic fields from cosmological phase transitions, *Phys. Lett. B* 265 (1991) 258–261.
 - [34] T. W. B. Kibble, A. Vilenkin, Phase equilibration in bubble collisions, *Phys. Rev. D* 52 (1995) 679–688.
 - [35] J. Ahonen, K. Enqvist, Magnetic field generation in first order phase transition bubble collisions, *Phys. Rev. D* 57 (1998) 664–673.
 - [36] M. Joyce, M. E. Shaposhnikov, Primordial magnetic fields, right electrons, and the Abelian anomaly, *Phys. Rev. Lett.* 79 (1997) 1193–1196.
 - [37] K. Takahashi, K. Ichiki, H. Ohno, H. Hanayama, Magnetic field generation from cosmological perturbations, *Phys. Rev. Lett.* 95 (2005) 121301.

- [38] H. Hanayama, et al., Biermann mechanism in primordial supernova remnant and seed magnetic fields, *Astrophys. J.* 633 (2005) 941.
- [39] K. Ichiki, K. Takahashi, H. Ohno, H. Hanayama, N. Sugiyama, Cosmological magnetic field: a fossil of density perturbations in the early universe, *Science* 311 (2006) 827.
- [40] F. Govoni, L. Feretti, Magnetic Fields in Clusters of Galaxies, *International Journal of Modern Physics D* 13 (2004) 1549–1594.
- [41] A. M. Wolfe, K. M. Lanzetta, A. L. Oren, Magnetic fields in damped Ly-alpha systems, *Astrophys. J.* 388 (1992) 17–22.
- [42] T. E. Clarke, P. P. Kronberg, H. Boehringer, A new radio - x-ray probe of galaxy cluster magnetic fields, *Astrophys. J.* 547 (2001) L111–L114.
- [43] Y. Xu, P. P. Kronberg, S. Habib, Q. W. Dufton, A faraday rotation search for magnetic fields in large scale structure, *Astrophys. J.* 637 (2006) 19–26.
- [44] D. J. Barnes, D. Kawata, K. Wu, Cosmological Simulations using GCMHD+, *ArXiv e-prints* arXiv:1112.0340.
- [45] A. R. Liddle, D. H. Lyth, *Cosmological Inflation and Large-Scale Structure*, Cambridge University Press, 2000.
- [46] D. Lemoine, M. Lemoine, Primordial magnetic fields in string cosmology, *Phys. Rev. D* 52 (4) (1995) 1955–1962.
- [47] J. M. Quashnock, A. Loeb, D. N. Spergel, Magnetic field generation during the cosmological qcd phase transition, *Astrophys. J. Lett.* 344 (1989) L49–L51.
- [48] G. Baym, D. Bödeker, L. McLerran, Magnetic fields produced by phase transition bubbles in the electroweak phase transition, *Phys. Rev. D* 53 (1996) 662–667.
- [49] C. Caprini, R. Durrer, Gravitational wave production: A strong constraint on primordial magnetic fields, *Phys. Rev. D* 65 (2001) 023517.

- [50] M. Maggiore, Gravitational wave experiments and early universe cosmology, *Physics Reports* 331 (2000) 283–367. [arXiv:arXiv:gr-qc/9909001](#), [doi:10.1016/S0370-1573\(99\)00102-7](#).
- [51] R. H. Cyburt, B. D. Fields, K. A. Olive, E. Skillman, New BBN limits on physics beyond the standard model from ^4He , *Astroparticle Physics* 23 (2005) 313–323. [arXiv:arXiv:astro-ph/0408033](#), [doi:10.1016/j.astropartphys.2005.01.005](#).
- [52] G. Hinshaw, M. R. Nolta, C. L. Bennett, R. Bean, O. Doré, M. R. Greason, M. Halpern, R. S. Hill, N. Jarosik, A. Kogut, E. Komatsu, M. Limon, N. Odegard, S. S. Meyer, L. Page, H. V. Peiris, D. N. Spergel, G. S. Tucker, L. Verde, J. L. Weiland, E. Wollack, E. L. Wright, Three-Year Wilkinson Microwave Anisotropy Probe (WMAP) Observations: Temperature Analysis, *Astrophys. J. Suppl* 170 (2007) 288–334.
- [53] L. Page, G. Hinshaw, E. Komatsu, M. R. Nolta, D. N. Spergel, C. L. Bennett, C. Barnes, R. Bean, O. Doré, J. Dunkley, M. Halpern, R. S. Hill, N. Jarosik, A. Kogut, M. Limon, S. S. Meyer, N. Odegard, H. V. Peiris, G. S. Tucker, L. Verde, J. L. Weiland, E. Wollack, E. L. Wright, Three-Year Wilkinson Microwave Anisotropy Probe (WMAP) Observations: Polarization Analysis, *Astrophys. J. Suppl* 170 (2007) 335–376.
- [54] D. N. Spergel, R. Bean, O. Doré, M. R. Nolta, C. L. Bennett, J. Dunkley, G. Hinshaw, N. Jarosik, E. Komatsu, L. Page, H. V. Peiris, L. Verde, M. Halpern, R. S. Hill, A. Kogut, M. Limon, S. S. Meyer, N. Odegard, G. S. Tucker, J. L. Weiland, E. Wollack, E. L. Wright, Three-Year Wilkinson Microwave Anisotropy Probe (WMAP) Observations: Implications for Cosmology, *Astrophys. J. Suppl* 170 (2007) 377–408.
- [55] E. Komatsu, J. Dunkley, M. R. Nolta, C. L. Bennett, B. Gold, G. Hinshaw, N. Jarosik, D. Larson, M. Limon, L. Page, D. N. Spergel, M. Halpern, R. S. Hill, A. Kogut, S. S. Meyer, G. S. Tucker, J. L. Weiland, E. Wollack, E. L. Wright, Five-Year Wilkinson Microwave Anisotropy Probe Observations: Cosmological Interpretation, *Astrophys. J. Suppl* 180 (2009) 330–376.
- [56] A. J. Ross, R. J. Brunner, A. D. Myers, Normalization of the Matter

- Power Spectrum via Higher Order Angular Correlations of Luminous Red Galaxies, *Astrophys. J.* 682 (2008) 737–744.
- [57] E. Rozo, et al., Cosmological Constraints from SDSS maxBCG Cluster Abundances [arXiv:astro-ph/0703571](#).
- [58] E. Komatsu, K. M. Smith, J. Dunkley, C. L. Bennett, B. Gold, G. Hinshaw, N. Jarosik, D. Larson, M. R. Nolta, L. Page, D. N. Spergel, M. Halpern, R. S. Hill, A. Kogut, M. Limon, S. S. Meyer, N. Odegard, G. S. Tucker, J. L. Weiland, E. Wollack, E. L. Wright, Seven-year Wilkinson Microwave Anisotropy Probe (WMAP) Observations: Cosmological Interpretation, *Astrophys. J. Suppl* 192 (2011) 18–+. [arXiv:1001.4538](#), [doi:10.1088/0067-0049/192/2/18](#).
- [59] S. Wang, New primordial-magnetic-field limit from the latest LIGO S5 data, *Phys. Rev. D* 81 (2) (2010) 023002.
- [60] The LIGO Scientific Collaboration and The Virgo Collaboration, An upper limit on the stochastic gravitational-wave background of cosmological origin, *Nature* 460 (2009) 990.
- [61] T. Kahniashvili, A. G. Tevzadze, S. K. Sethi, K. Pandey, B. Ratra, Primordial magnetic field limits from cosmological data, *Phys. Rev. D* 82 (8) (2010) 083005.
- [62] D. Paoletti, F. Finelli, CMB constraints on a stochastic background of primordial magnetic fields, *Phys. Rev.* (12) (2011) 123533–+. [arXiv:1005.0148](#), [doi:10.1103/PhysRevD.83.123533](#).
- [63] J. Silk, Cosmic Black-Body Radiation and Galaxy Formation, *Astrophys. J.* 151 (1968) 459.
- [64] T. R. Seshadri, K. Subramanian, CMBR Polarization Signals from Tangled Magnetic Fields, *Phys. Rev. Lett.* 87 (2001) 101301.
- [65] A. A. Starobinskii, *ZhETF Pis ma Redaktsiiu* 30 (1979) 719.
- [66] V. A. Rubakov, M. V. Sazhin, A. V. Veryaskin, *Physics Letters B* 115 (1982) 189.
- [67] A. G. Polnarev, *Soviet Astronomy* 29 (1985) 607.

- [68] J. R. Pritchard, M. Kamionkowski, *Ann. Phys.* 318 (2005) 2.
- [69] R. A. Sunyaev, I. B. Zeldovich, Microwave background radiation as a probe of the contemporary structure and history of the universe, *ARA. and A.* 18 (1980) 537–560. doi:10.1146/annurev.aa.18.090180.002541.
- [70] A. Lewis, S. Bridle, Cosmological parameters from cmb and other data: a monte- carlo approach, *Phys. Rev. D* 66 (2002) 103511.
- [71] P. J. E. Peebles, *The Large-Scale Structure of the Universe*, Princeton University Press, 1980.
- [72] K. Yamamoto, N. Sugiyama, H. Sato, Evolution of small-scale cosmological baryon perturbations and matter transfer functions, *Astrophys. J.* 501 (1997) 442.
- [73] S. Cole, et al., The 2dF Galaxy Redshift Survey: Power-spectrum analysis of the final dataset and cosmological implications, *Mon. Not. Roy. Astron. Soc.* 362 (2005) 505–534.
- [74] M. Tegmark, et al., Cosmological Constraints from the SDSS Luminous Red Galaxies, *Phys. Rev. D* 74 (2006) 123507.
- [75] K. Jedamzik, V. Katalinic, A. V. Olinto, Damping of cosmic magnetic fields, *Phys. Rev. D* 57 (1998) 3264–3284.
- [76] K. Subramanian, J. D. Barrow, Magnetohydrodynamics in the early universe and the damping of nonlinear alfven waves, *Phys. Rev. D* 58 (1998) 083502.
- [77] R. Banerjee, K. Jedamzik, The evolution of cosmic magnetic fields: From the very early universe, to recombination, to the present, *Phys. Rev. D* 70 (2004) 123003.
- [78] J. Dunkley, et al., Five-Year Wilkinson Microwave Anisotropy Probe (WMAP) Observations: Likelihoods and Parameters from the WMAP data, *Astrophys. J. Suppl.* 180 (2009) 306–329.

- [79] F. Finelli, F. Paci, D. Paoletti, The Impact of Stochastic Primordial Magnetic Fields on the Scalar Contribution to Cosmic Microwave Background Anisotropies, *Phys. Rev. D* 78 (2008) 023510. [arXiv:0803.1246](#), [doi:10.1103/PhysRevD.78.023510](#).
- [80] J. R. Shaw, A. Lewis, Constraining Primordial Magnetism, *ArXiv e-prints* [arXiv:1006.4242](#).
- [81] G. Hinshaw, J. L. Weiland, R. S. Hill, N. Odegard, D. Larson, C. L. Bennett, J. Dunkley, B. Gold, M. R. Greason, N. Jarosik, E. Komatsu, M. R.olta, L. Page, D. N. Spergel, E. Wollack, M. Halpern, A. Kogut, M. Limon, S. S. Meyer, G. S. Tucker, E. L. Wright, Five-Year Wilkinson Microwave Anisotropy Probe Observations: Data Processing, Sky Maps, and Basic Results, *Astrophys. J* 180 (2009) 225–245.
- [82] C. L. Kuo, P. A. R. Ade, J. J. Bock, J. R. Bond, C. R. Contaldi, M. D. Daub, J. H. Goldstein, W. L. Holzapfel, A. E. Lange, M. Lueker, M. Newcomb, J. B. Peterson, C. Reichardt, J. Ruhl, M. C. Runyan, Z. Staniszewski, Improved measurements of the cmb power spectrum with acbar, *Astrophys. J.* 664 (2) (2007) 687–701.
- [83] J. L. Sievers, C. Achermann, J. R. Bond, L. Bronfman, R. Bustos, C. R. Contaldi, C. Dickinson, P. G. Ferreira, M. E. Jones, A. M. Lewis, B. S. Mason, J. May, S. T. Myers, N. Oyarce, S. Padin, T. J. Pearson, M. Pospieszalski, A. C. S. Readhead, R. Reeves, A. C. Taylor, S. Torres, Implications of the cosmic background imager polarization data, *Astrophys. J.* 660 (2007) 976–987.
- [84] W. C. Jones, et al., A measurement of the angular power spectrum of the cmb temperature anisotropy from the 2003 flight of boomerang, *Astrophys. J.* 647 (2006) 823–832.
- [85] J. R. Bond, G. Efstathiou, J. Silk, Massive neutrinos and the large-scale structure of the universe, *Physical Review Letters* 45 (1980) 1980–1984. [doi:10.1103/PhysRevLett.45.1980.2](#).
- [86] J. Lesgourgues, S. Pastor, Massive neutrinos and cosmology, *Phys. Rept.* 429 (2006) 307–379.
- [87] F. De Bernardis, P. Serra, A. Cooray, A. Melchiorri, An improved limit on the neutrino mass with CMB and redshift-dependent halo bias-mass

- relations from SDSS, DEEP2, and Lyman-Break Galaxies, *Phys. Rev. D* 78 (2008) 083535.
- [88] K. Ichiki, Y.-Y. Keum, Neutrino Masses from Cosmological Probes in Interacting Neutrino Dark-Energy Models, *JHEP* 06 (2008) 058.
 - [89] K. Ichiki, M. Takada, T. Takahashi, Constraints on Neutrino Masses from Weak Lensing [arXiv:0810.4921](#).
 - [90] E. W. Otten, C. Weinheimer, Neutrino mass limit from tritium β decay, *Reports on Progress in Physics* 71 (8) (2008) 086201–+. doi:10.1088/0034-4885/71/8/086201.
 - [91] O. Elgaroy, et al., A new limit on the total neutrino mass from the 2dF galaxy redshift survey, *Phys. Rev. Lett.* 89 (2002) 061301.
 - [92] E. Komatsu, A. Kogut, M. R.olta, C. L. Bennett, M. Halpern, G. Hinshaw, N. Jarosik, M. Limon, S. S. Meyer, L. Page, D. N. Spergel, G. S. Tucker, L. Verde, E. Wollack, E. L. Wright, First-Year Wilkinson Microwave Anisotropy Probe (WMAP) Observations: Tests of Gaussianity, *Astrophys. J. Suppl* 148 (2003) 119–134.
 - [93] M. Shiraishi, D. Nitta, S. Yokoyama, K. Ichiki, K. Takahashi, Cosmic microwave background bispectrum of tensor passive modes induced from primordial magnetic fields, *Phys. Rev. D* 83 (12) (2011) 123003.
 - [94] P. Trivedi, K. Subramanian, T. R. Seshadri, Primordial magnetic field limits from cosmic microwave background bispectrum of magnetic passive scalar modes, *Phys. Rev. D* 82 (12) (2010) 123006.
 - [95] C. Caprini, F. Finelli, D. Paoletti, A. Riotto, The cosmic microwave background temperature bispectrum from scalar perturbations induced by primordial magnetic fields, *JCAP* 6 (2009) 21.
 - [96] T. R. Seshadri, K. Subramanian, Cosmic Microwave Background Bispectrum from Primordial Magnetic Fields on Large Angular Scales, *Physical Review Letters* 103 (8) (2009) 081303.
 - [97] I. Brown, R. Crittenden, Non-Gaussianity from cosmic magnetic fields, *Phys. Rev. D* 72 (6) (2005) 063002.

- [98] H. Tashiro, N. Sugiyama, Probing primordial magnetic fields with the 21-cm fluctuations, *Mon. Not. Roy. Astron. Soc.* 372 (2006) 1060–1068.

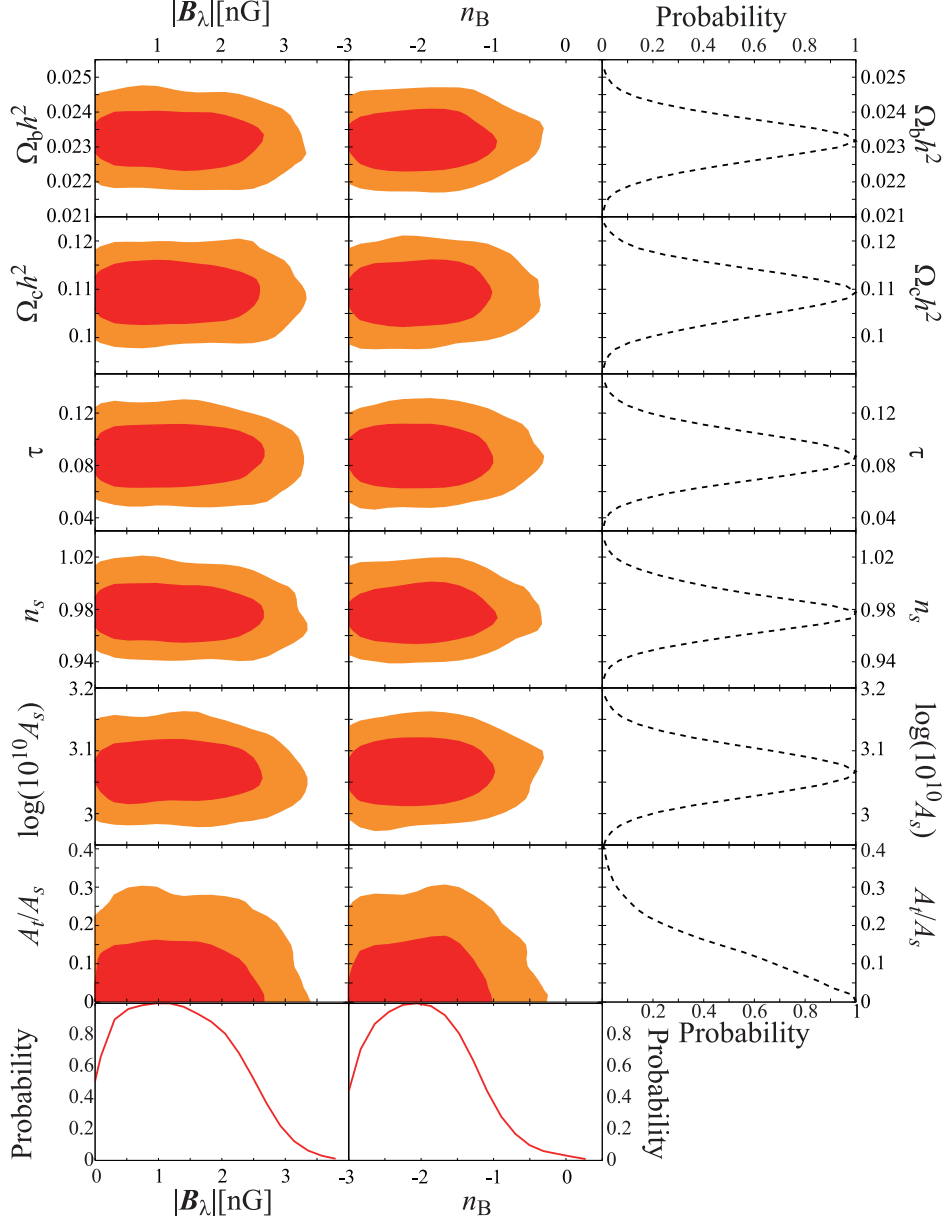


Figure 7: Probability contour plane of PMF parameters (n_B and B_λ) vs. the standard cosmological parameters and probability distributions for PMF parameters and the standard cosmological parameters. Deep (red) and pale (orange) contours show the 1σ (68%) and 2σ (95%) confidence limits. Bold (red) curves on the bottom of the figure are the probability distributions for the PMF parameters. Dashed (black) curves on the right of the figure are the probability distributions of each standard cosmological parameter. (For interpretation of the references to colour in this figure legend, the reader is referred to the web version of this article.)

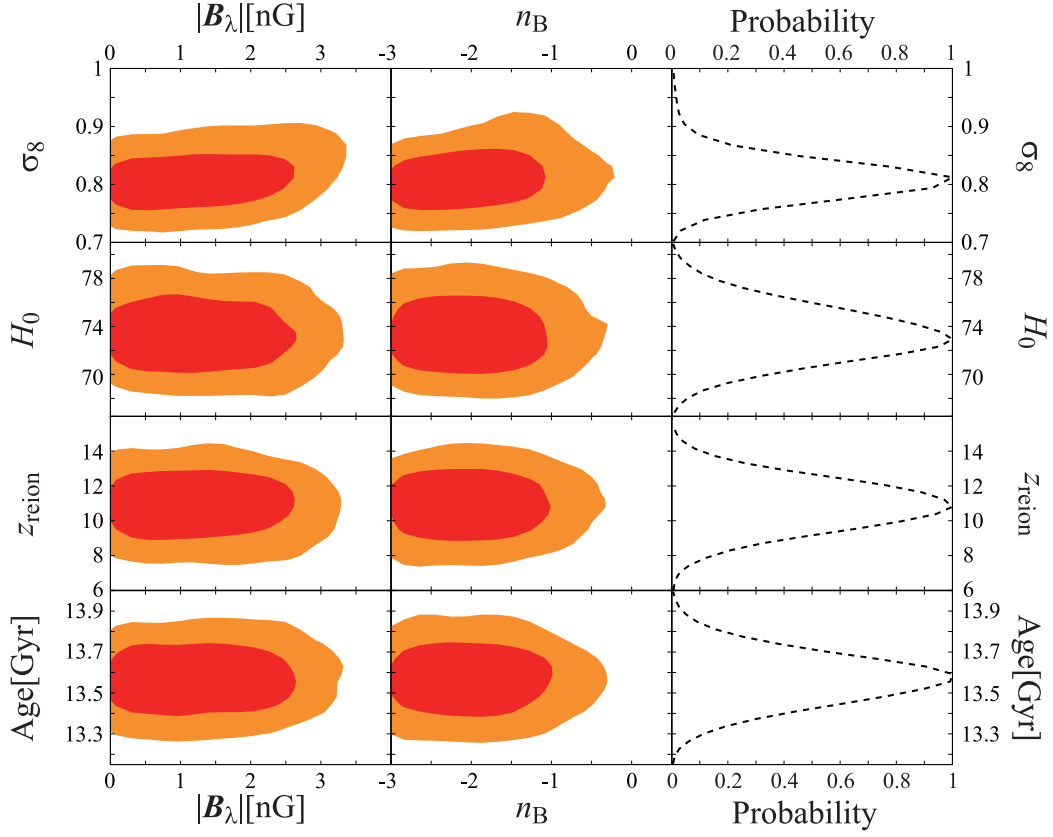


Figure 8: Probability contour plane of PMF parameters (n_B and B_λ) vs. the derived parameters σ_8 , H_0 , z_{reion} and Age and probability distributions for the derived parameters. Deep (red) and pale (orange) contours show the 1σ (68%) and 2σ (95%) confidence limits. Dashed (black) curves on the right of the figure are the probability distributions for each derived parameter. (For interpretation of the references to colour in this figure legend, the reader is referred to the web version of this article.)

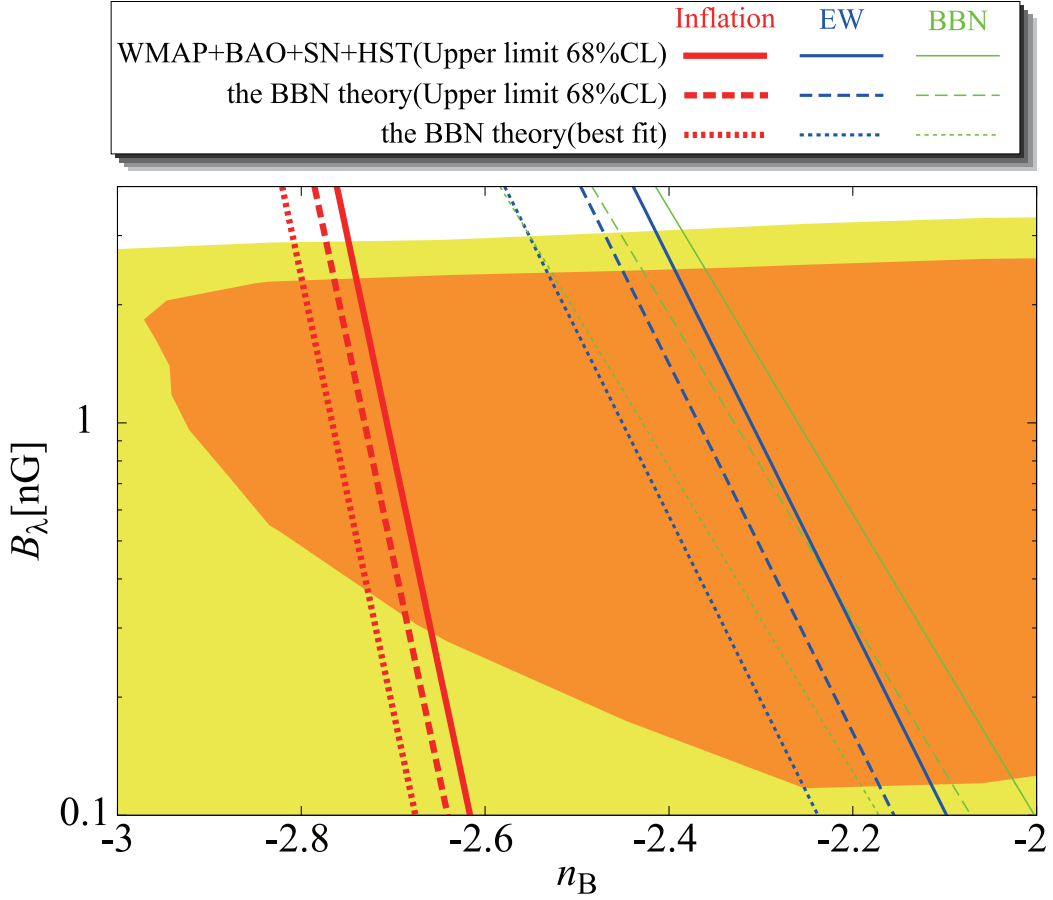


Figure 9: Allowed and excluded regions in the 1σ (68%) C.L. and 2σ (95.4%) C.L. in the plane of $|B_\lambda|$ vs. n_B obtained by an MCMC method applied to the CMB (WMAP 5yr [81], ACBAR[82], CBI[83], Boomerang [84]) and the LSS (2dFDR [73]) observational data. The thin (green), middle (blue), and bold (red) lines show upper limits on the produced PMF during the epoch of BBN, the electroweak transition, and the inflation epoch, respectively. (For interpretation of the references to colour in this figure legend, the reader is referred to the web version of this article.)

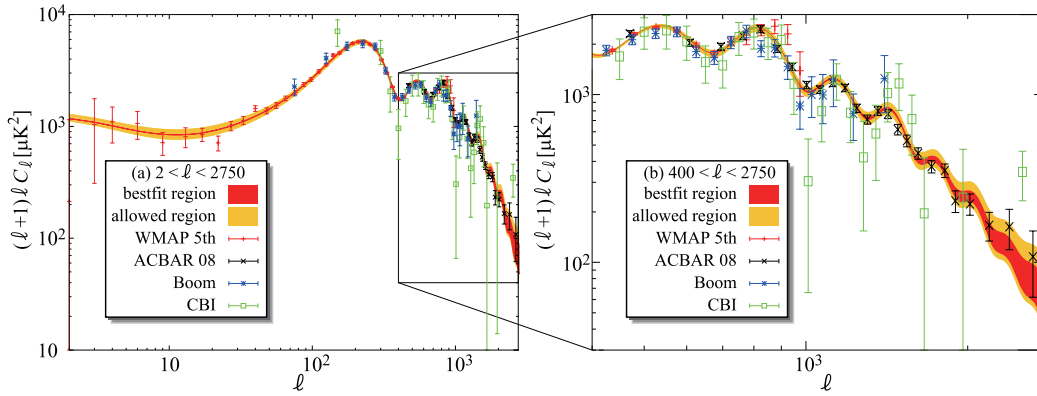


Figure 10: Comparison of the observed CMB with the computed total TT power spectra from the best-fit and allowed parameters. Various ranges of each plots are (a) TT($2 < \ell < 2750$) and (b) TT($400 < \ell < 2750$). Deep colour (red) regions indicate the best-fit parameter set and allowed regions [pale (orange) colour] are from the constrained parameter set of Table.1. Dots with error bars show the WMAP 5yr, ACBAR 08, Boomerang and CBI data as the legend box in each panel. The upper curves of allowed regions in each panel include the SZ effect at the K(22.8GHz) band, and the lower curves do not include the SZ effect. (For interpretation of the references to colour in this figure legend, the reader is referred to the web version of this article.) (For interpretation of the references to colour in this figure legend, the reader is referred to the web version of this article.)

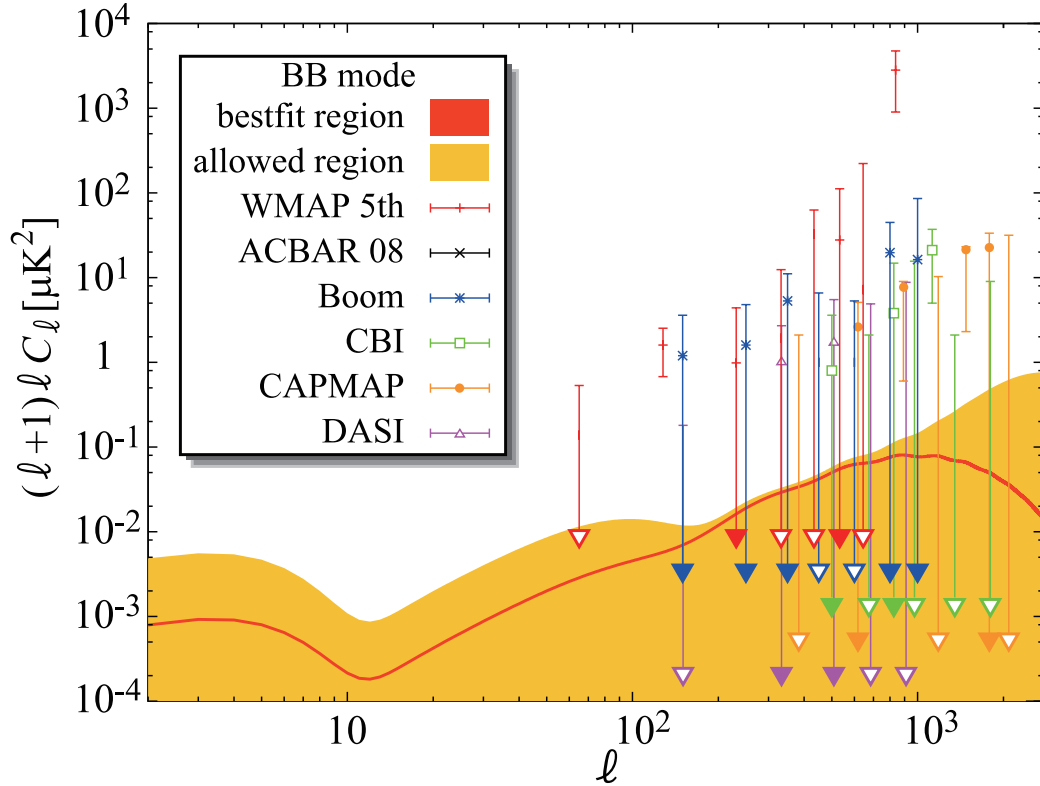


Figure 11: Comparison of the observed CMB with the computed total BB power spectra from the best-fit and allowed parameters. Deep colour (red) regions indicate the best-fit parameter set and allowed regions [pale (orange) colour] are from the constrained parameter set of Table.1. Dots with error bars show the WMAP 5yr, ACBAR 08, Boomerang, CBI, CAPMAP, and DASI data as the legend box in the figure. Downward arrows for the error bars indicate that the data points are upper limits. (For interpretation of the references to colour in this figure legend, the reader is referred to the web version of this article.)

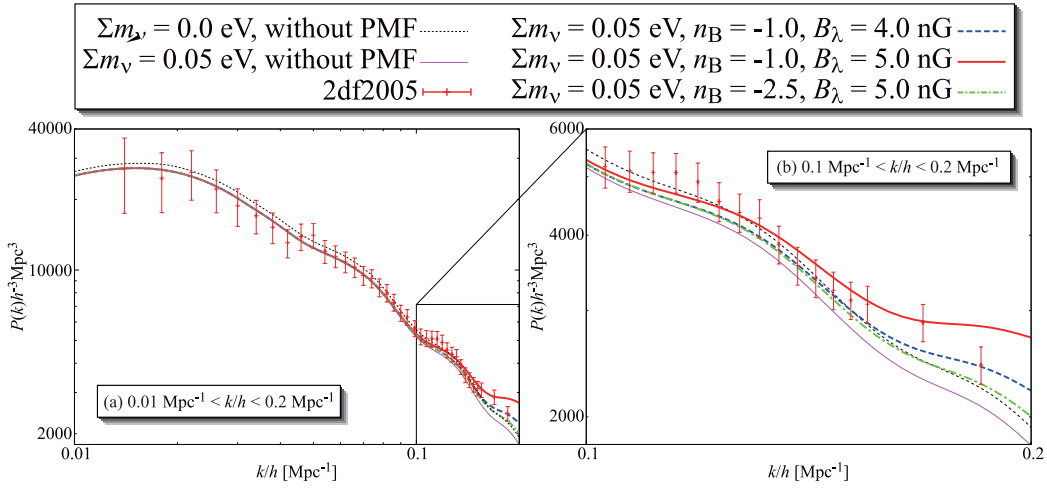


Figure 12: Matter power spectra from finite mass neutrinos and a PMF. The range of the left and right panel is $0.01\text{Mpc}^{-1}k/h < 0.2\text{Mpc}^{-1}$ and $0.1\text{Mpc}^{-1}k/h < 0.2\text{Mpc}^{-1}$. Dots with error bars and curves are as indicated in the legend box in the figure. To better illustrate effects of finite-mass neutrinos and a PMF for the matter power spectra, we have used a larger field strength of a PMF B_λ . This figure shows that a PMF affects strongly the matter power spectra on $k/h > 0.1\text{Mpc}^{-1}$. The magnitude of PMF effect depends on both B_λ and n_B . On one hand, the total amplitudes of the matter power spectra are decreased by the neutrino mass. Furthermore, the effects from the mass of neutrinos on larger k (smaller scales) are greater than on smaller k (larger scales).

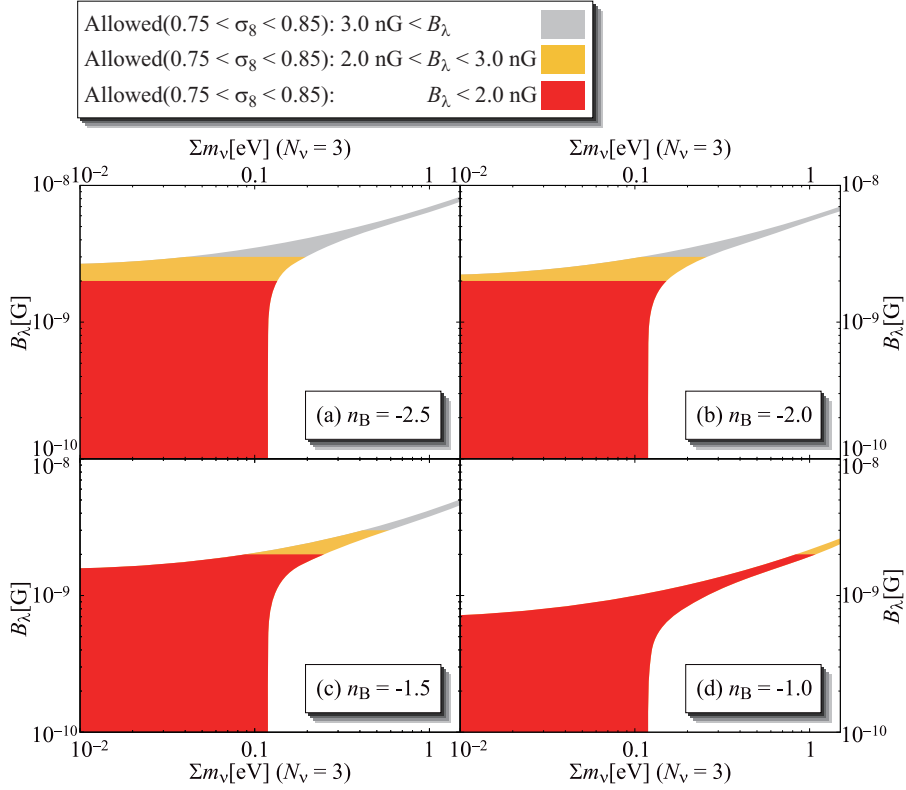


Figure 13: Allowed and excluded regions for the σ_8 on the B_λ vs. $\sum_{N_\nu=3} m_\nu$ plane. Filled regions indicate ranges of σ_8 as $0.75 < \sigma_8 < 0.85$ and pale colour (gray), middle colour (yellow) and deep colour (red) regions show $B_\lambda > 3.0$ nG, $B_\lambda < 3.0$ nG and $B_\lambda < 2.0$ nG, respectively. (For interpretation of the references to colour in this figure legend, the reader is referred to the web version of this article.)